UNIVERSITY OF CALIFORNIA, SAN DIEGO

Evidence of a new boson that decays to two W bosons in the full leptonic final states in 24.4 fb^{-1} at center-of-mass energy of 7 and 8 TeV with Compact Muon Solenoid detector

A dissertation submitted in partial satisfaction of the
requirements for the degree
Doctor of Philosophy

in

Physics

by

Jae Hyeok Yoo

Committee in charge:

Professor Frank Würthwein, Chair
Professor Claudio Campagnari
Professor Pamela Cosman
Professor Aneesh Manohar
Professor Avraham Yagil

2013

The dissertation of Jae Hyeok Yoo is approved, and it is acceptable in quality and form for publication on microfilm and electronically:

____

____

____

____

Chair

University of California, San Diego

2013

DEDICATION

To two, the loneliest number since the number one.

EPIGRAPH

A careful quotation
conveys brilliance.
—Smarty Pants

TABLE OF CONTENTS

ACKNOWLEDGEMENTS

Thanks to whoever deserves credit for Blacks Beach, Porters Pub, and every coffee shop in San Diego.

Thanks also to hottubs.

VITA

2007	B.S. in Physics, Korea University
2009	M.S. in Physics, Korea University
2013	Ph.D. in Physics, University of California, San Diego

PUBLICATIONS

Your Name, “A Simple Proof Of The Riemann Hypothesis”, *Annals of Math*, 314, 2007.

Your Name, Euclid, “There Are Lots Of Prime Numbers”, *Journal of Primes*, 1, 300 B.C.

ABSTRACT OF THE DISSERTATION

Evidence of a new boson that decays to two W bosons in the full leptonic final states in 24.4 fb^{-1} at center-of-mass energy of 7 and 8 TeV with Compact Muon Solenoid detector

by

Jae Hyeok Yoo

Doctor of Philosophy in Physics

University of California, San Diego, 2013

Professor Frank Würthwein, Chair

This dissertation will be abstract.

Chapter 1

Higgs Boson in Standard Model

1.1 Higgs Mechanism

Properties of elementary particles in nature and their interactions (forces) to each other are described by Standard Model (SM) in particle physics. It is based on the gauge symmetry and the group sturucture of $\mathrm{SU(3)_c} \otimes \mathrm{SU(2)_L} \otimes \mathrm{U(1)_Y}$, where $\mathrm{SU(3)_c}$, $\mathrm{SU(2)_L}$ and $\mathrm{U(1)_Y}$ describe color, weak isospin and hyper charge, respectively. The gauge symmetry requires the weak gauge bosons to be massless, but experimentally we know that Weak gauge bosons, $W^{\pm}$ and Z are massive. The cure for this is the Higgs mechanism [] based on the spontanesous symmetry breaking(SSB) which breaks $\mathrm{SU(2)_L} \otimes \mathrm{U(1)_Y}$ to $\mathrm{U(1)_{EM}}$, thus gives masses to weak bosons but keeps photon massless.

1.1.1 How particles become massive : Higgs Mechanism

Since Electroweak(EWK) theory is based on SU(2) symmetry, the Higgs field is given as a SU(2) doublet,

$$\phi = \begin{pmatrix} \phi^+ \\ \phi^0 \end{pmatrix} \tag{1.1}$$

where each element is a complex field,

$$\phi^+ = \frac{\phi_1 + i\phi_2}{\sqrt{2}} \qquad \text{and} \qquad \phi^0 = \frac{\phi_3 + i\phi_4}{\sqrt{2}}. \tag{1.2}$$

We start with the Higgs Lagrangian to understand the essence of spontanesous symmetry breaking(SSB) before making the things more complicated. The full SM Lagrangian will be discussed later. The Higgs Lagrangian($\mathcal{L}_\phi$) is composed of the kinetic and the potential terms.

$$\mathcal{L}_\phi = \underbrace{(\partial_\mu \phi)^\dagger (\partial^\mu \phi)}_{\text{kinetic term}} - \underbrace{\left(\mu^2 \phi^\dagger \phi + \lambda \left(\phi^\dagger \phi\right)^2\right)}_{\text{potential}} \tag{1.3}$$

where $\mu^2 < 0$ and $\lambda > 0$. The potential term which is a function of $\phi^\dagger \phi$ is invariant under SU(2) local gauge transformation,

$$\phi(x) \to \phi(x)' = e^{i\vec{\alpha}(x)\cdot\frac{\vec{\sigma}}{2}} \phi(x), \tag{1.4}$$

where $\vec{\alpha}(x)$ is a vector of parameters and $\vec{\sigma}$ is a vector of Pauli matrice,

$$\sigma_1 = \begin{pmatrix} 0 & 1 \\ 1 & 0 \end{pmatrix}, \quad \sigma_2 = \begin{pmatrix} 0 & -i \\ i & 0 \end{pmatrix} \quad \text{and} \quad \sigma_3 = \begin{pmatrix} 1 & 0 \\ 0 & -1 \end{pmatrix}.$$

The potential has the minimum at $\phi^\dagger\phi = -\mu^2/2\lambda = v^2/2$ where v is the vacuum expectation value of the Higgs field ϕ. Due to SU(2) symmetry, the choice of vacuum state is not definite as seen in the following equation,

$$\phi^\dagger\phi = \frac{1}{2}\left(\phi_1^2 + \phi_2^2 + \phi_3^2 + \phi_4^2\right) = \frac{v^2}{2} \tag{1.5}$$

where there are 4 real variables with only one contraint. This leads to an appropriate choice of vacuum for the physics of interest. We choose the vacuum state, ϕ_0, as

$$\phi_0 = \frac{1}{\sqrt{2}}\begin{pmatrix} 0 \\ v \end{pmatrix} \tag{1.6}$$

and expand around it by $H(x)$

$$\phi(x) = \frac{1}{\sqrt{2}}\begin{pmatrix} 0 \\ v + H(x) \end{pmatrix} \tag{1.7}$$

where $H(x)$ is the physical Higgs field. In order to make the lagrangian invariant under SU(2) transformation, the derivative ∂_μ should be replaced by the covariant derivative $\mathcal{D}_\mu$,

$$\mathcal{D}_\mu = \partial_\mu - ig_1\frac{Y}{2}B_\mu - ig_2\frac{\vec{\sigma}}{2}\cdot\overrightarrow{W}_\mu. \tag{1.8}$$

B_μ and $\overrightarrow{W}_\mu$ are the vector fields needed for U(1) and SU(2) gauge invariance, respectively. The g_1 and g_2 are the couplings that decide the strength of the interactions associated with B_μ and $\overrightarrow{W}_\mu$. Y(weak hypercharge) and $\vec{\sigma}/2$ are the generators for U(1) and SU(2), respectively. Putting this into the Lagrangian $\mathcal{L}_\phi$, the kinetic term contains

$$\phi^\dagger\left[-ig_1\frac{Y}{2}B^\mu - ig_2\frac{\vec{\sigma}}{2}\cdot\overrightarrow{W}^\mu\right]^\dagger\left[-ig_1\frac{Y}{2}B^\mu - ig_2\frac{\vec{\sigma}}{2}\cdot\overrightarrow{W}^\mu\right]\phi. \tag{1.9}$$

In order to derive the masses of W and Z bosons, we use the vacuum state of Higgs field ϕ_0 because masses are present even without dynamical fields. With $Y = 1$ and $\phi = \frac{1}{\sqrt{2}}\begin{pmatrix} 0 \\ v \end{pmatrix}$, and writing explicitly in 2×2 matrices, eq. (1.9) becomes

$$\begin{aligned}
&\frac{1}{8}\left|\begin{pmatrix} g_1 B_\mu + g_2 W_\mu^3 & g_2(W_\mu^1 - iW_\mu^2) \\ g_2(W_\mu^1 + iW_\mu^2) & g_1 B_\mu - g_2 W_\mu^3 \end{pmatrix}\begin{pmatrix} 0 \\ v \end{pmatrix}\right|^2 \\
&\qquad = \frac{v^2}{8}\left|\begin{pmatrix} g_2(W_\mu^1 - iW_\mu^2) \\ g_1 B_\mu - g_2 W_\mu^3 \end{pmatrix}\right|^2 \qquad (1.10)\\
&\qquad = \frac{v^2 g_2^2}{8}\left[\left(W_\mu^1\right)^2 + \left(W_\mu^2\right)^2\right] + \frac{v^2}{8}\left(g_1 B_\mu - g_2 W_\mu^3\right)^2.
\end{aligned}$$

The first term can be re-written using charge states, $W^\pm = \frac{1}{\sqrt{2}}\left(W^1 \mp iW^2\right)$,

$$\frac{1}{2}\left(\frac{v g_2}{2}\right)^2\left[\left(W_\mu^+\right)^2 + \left(W_\mu^-\right)^2\right]. \qquad (1.11)$$

Thus, we have the mass of charged W boson $M_W = \frac{v g_2}{2}$. Now we know that the second term in eq. (1.10) should correspond to Z boson because that is the only remaining massive boson. Imposing the same normalization to the mixed field as the unmixed fields, the physical field for Z boson, Z_μ, is given by

$$Z_\mu = \frac{\left(g_1 B_\mu - g_2 W_\mu^3\right)}{\sqrt{g_1^2 + g_2^2}} \qquad (1.12)$$

which gives its mass, $M_Z = \frac{v}{2}\sqrt{g_1^2 + g_2^2}$.

There is a massless field orthogonal to Z_μ,

$$A_\mu = \frac{\left(g_1 B_\mu + g_2 W_\mu^3\right)}{\sqrt{g_1^2 + g_2^2}} \qquad (1.13)$$

It does not appear in the Lagrangian because its mass therm is zero. This is the field that remains unbroken by SSB. So, it corresponds to photon.

Re-writing the potential term in eq. (1.3) using the physical weak boson states, $W_\mu^\pm$ and Z_μ, and their masses, we have the following terms for interactions between Higgs and weak bosons,

$$
\begin{aligned}
2\frac{M_W^2}{v}H(x)W_\mu^+W_\mu^- + \frac{M_Z^2}{v}H(x)\left(Z_\mu\right)^2 \\
+\frac{M_W^2}{v^2}H(x)^2W_\mu^+W_\mu^- + \frac{M_Z^2}{2v^2}H(x)^2\left(Z_\mu\right)^2 .
\end{aligned}
\tag{1.14}
$$

For Higgs-Weak boson interactions, the couplings are proportional to the square of weak boson mass. The corresponding Feynman diagrams are shown in Fig 1.1.

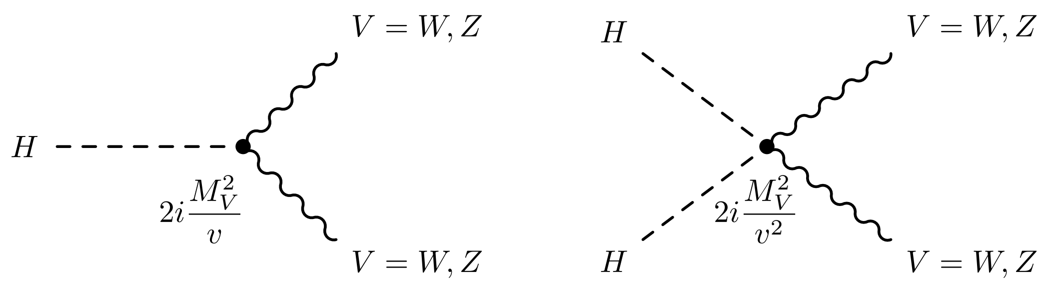

(a) H-VV interaction

(b) HH-VV interaction

Figure 1.1: Feynman diagrams for (a) H-VV and (b) HH-VV interactions.

Considering additional factorials due to identical particles, the vertex factors can be written as $2i\frac{M_V^2}{v}$ and $2i\frac{M_V^2}{v^2}$ for H-VV and HH-VV vertices, respectively, where V denotes W or Z.

After SSB, the Higss potential term, $\mu^2\phi^\dagger\phi + \lambda\left(\phi^\dagger\phi\right)^2$, in the Lagrangian becomes

$$
\begin{aligned}
\mathcal{L}_{\text{Higgs Potential}} &= \mu^2\phi^\dagger\phi + \lambda\left(\phi^\dagger\phi\right)^2 && (1.15)\\
&= \frac{\mu^2}{2}(v+H)^2 + \frac{\lambda}{4}(v+H)^4 && (1.16)\\
&= ... - \mu^2H^2 - \frac{\mu^2}{v}H^3 - \frac{\mu^2}{4v^2}H^4 && (1.17)
\end{aligned}
$$

where H^0 and H^1 terms are ignored in the last line because they are irrelevant in S-matrix calculations. From eq. (1.17), the Higgs mass is identified as $m_{\mathrm{H}}^2 = -2\mu^2$. Using this definition, eq. (1.17) becomes

$$
\mathcal{L}_{\text{Higgs Potential}} = ... - \frac{1}{2}m_{\mathrm{H}}^2H^2 - \frac{m_{\mathrm{H}}^2}{2v}H^3 - \frac{m_{\mathrm{H}}^2}{8v^2}H^4 \tag{1.18}
$$

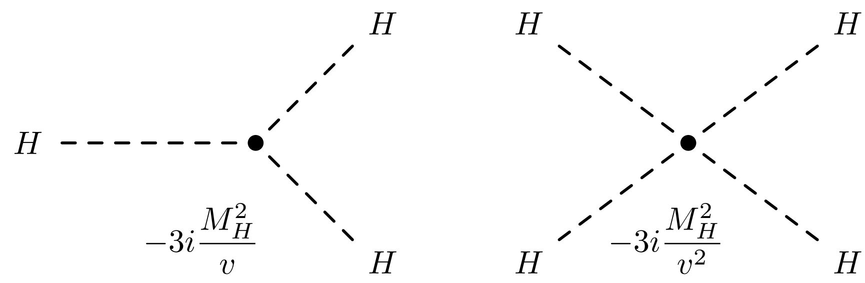

(a) HHH interaction (b) HHHH interaction

Figure 1.2: Feynman diagrams for (a) H^3 and (b) H^4 interactions.

The corresponding Feynman diagrams are shown in Fig 1.2.

Now we see that the entire Higgs sector depends on only m_{H} and v. The v is calculated by $v = \left(\sqrt{2}\mathrm{G_F}\right)^{-1/2} = 246$ GeV where $\mathrm{G_F}$ is the Fermi contant which is extracted from measurement of muon lifetime. Thus, the SM Higgs sector is fully described by m_{H}. m_{H} is a fuction of λ and $v(m_{\mathrm{H}}^2 = 2\lambda v^2)$ and we do not know the physical meaning of λ, so the mass of Higgs boson is not predictable by theory. It's experimentalists' task to measure m_{H} and complete the Standard Model of particle physics.

The introduced Higgs field had 4 degrees of freedom, ϕ_1, ϕ_2, ϕ_3 and ϕ_4 before SSB. But, we chose the Higgs field to have only one degree of freedom, $H(x)$. Where did the three go? By breaking $\mathrm{SU(2)_L} \otimes \mathrm{U(1)_Y}$ to $U(1)_{EM}$, the three gauge bosons acquired masses. This was done by adding longitudinal components to the three gauge bosons. As a result, we have only one physical Higgs field and three massive and one massless gauge bosons, instead of four unphysical Higgs fields and four massless gauge bosons.

The fermions acquire their masses by interacting with Higgs field. Let's start a discusstion with leptons because the absence of right-handed neutrinos, *i.e.* neutrinos are massless, makes the case simpler than quarks which have both right-handed and left-handed polarizations. Tab. 1.1.1 shows the quantum numbers of $\mathrm{SU(2)_L} \otimes \mathrm{U(1)_Y}$ for the left-handed electron doublet, right-handed neutrino, right-

	T_3	Y
$\begin{pmatrix} \nu_L \\ e_L \end{pmatrix}$	$\frac{1}{2}$	-1
ν_R	0	0
e_R	0	-2
$\begin{pmatrix} \phi_+ \\ \phi_0 \end{pmatrix}$	$\frac{1}{2}$	-1

Table 1.1: $\mathrm{SU(2)_L} \otimes \mathrm{U(1)_Y}$ quantum numbers

handed electron and Higgs doublet. Electron can be replaced by muon or tau leptons. From the table, one can see that the interaction such as

$$e_R + \begin{pmatrix} \phi_+ \\ \phi_0 \end{pmatrix} \to \begin{pmatrix} \nu_L \\ e_L \end{pmatrix} \tag{1.19}$$

conserves quantum numbers. Now the structure of the interaction is given, and we specify its strength with g_e. Including the hermitian conjugate to the Lagrangian, the lepton-Higgs interaction term becomes

$$\mathcal{L}_{int,lepton} = -g_e \left[\begin{pmatrix} \bar{\nu}_L & \bar{e}_L \end{pmatrix} \begin{pmatrix} \phi_+ \\ \phi_0 \end{pmatrix} e_R + \bar{e}_R \begin{pmatrix} \bar{\phi}_+ & \bar{\phi}_0 \end{pmatrix} \begin{pmatrix} \nu_L \\ e_L \end{pmatrix} \right] \tag{1.20}$$

Using the chosen Higgs field in eq. (1.7), the Lagrangian is calculated to be

$$\mathcal{L}_{int,lepton} = -\frac{g_e v}{\sqrt{2}} \left(\bar{e}_L e_R + \bar{e}_R e_L \right) - \frac{g_e H}{\sqrt{2}} \left(\bar{e}_L e_R + \bar{e}_R e_L \right). \tag{1.21}$$

Since $\bar{e}e = \bar{e}(P_L^2 + P_R^2)e = \bar{e}_L e_R + \bar{e}_R e_L$ where P_L and P_R are projection operators, the first term, $-\frac{g_e v}{\sqrt{2}}\bar{e}e$, corresponds to the mass term for the electron. Thus, the mass is identified to be

$$m_e = \frac{g_e v}{\sqrt{2}}. \tag{1.22}$$

Rewriting the Lagrangian in terms of m_e instead of an arbitary g_e, we get

$$\mathcal{L}_{int} = -m_e \bar{e}e - \frac{m_e}{v}\bar{e}eH. \tag{1.23}$$

Since there isn't a physical motivation for g_e, m_e is not calculable by theory, but needs to be determined by experiments. The second term corresponds to lepton-Higgs interaction. The size of the interaction is proportional to the mass of electrons. Thus, light leptons have very weak couplings to the Higgs field. For example, electron has $\frac{m_e}{v}$ = 0.5 MeV/246 GeV $\sim \mathcal{O}\left(10^{-6}\right)$ and muon has 106 MeV/246 GeV $\sim \mathcal{O}\left(10^{-3}\right)$.

The case for quarks is more complicated due to the presence of right-handed up-type quarks as opposed to the lepton case. In order to generate masses for up-type quarks, we need a new Higgs doublet

$$\phi_c = i\sigma_2\phi^* = \begin{pmatrix} \phi_0^* \\ -\phi_- \end{pmatrix} = \frac{1}{\sqrt{2}}\begin{pmatrix} v + H(x) \\ 0 \end{pmatrix}. \tag{1.24}$$

The new Higgs field is invariant under $\mathrm{SU(2)_L}$ transformation and has Y = -1.

$$\begin{aligned} \mathcal{L}_{int,quark} &= -g_d\left[\begin{pmatrix} \bar{u}_L & \bar{d}_L \end{pmatrix}\begin{pmatrix} \phi_+ \\ \phi_0 \end{pmatrix} d_R\right] \\ &\qquad -g_u\left[\begin{pmatrix} \bar{u}_L & \bar{d}_L \end{pmatrix}\begin{pmatrix} \phi_0^* \\ -\phi_+ \end{pmatrix} u_R\right] + h.c. && (1.25) \\ &= -\frac{g_d v}{\sqrt{2}}\bar{d}d - \frac{g_d H}{\sqrt{2}}\bar{d}d - \frac{g_u v}{\sqrt{2}}\bar{u}u - \frac{g_u H}{\sqrt{2}}\bar{u}u && (1.26) \\ &= -m_d\bar{d}d - \frac{m_d}{v}\bar{d}dH - m_u\bar{u}u - \frac{m_u}{v}\bar{u}uH && (1.27) \end{aligned}$$

where u and d are up-type and down-type quarks, respectivley, and

$$m_d = \frac{g_d v}{\sqrt{2}} \quad \text{and} \quad m_u = \frac{g_u v}{\sqrt{2}} \tag{1.28}$$

are used as the lepton case.

As a result, the strength of interaction depends on the fermion mass, m_f/v. Fig. 1.3 shows Feynman diagram for Higgs - fermion interaction.

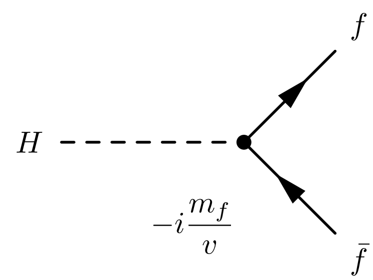

Figure 1.3: Feynman diagram for Hff interaction.

1.2 Production and Decay of Higgs Boson

1.2.1 Production of Higgs Boson

Standard model Higgs boson is generated by 4 major processes, gluon-gluon fusion (ggH : $gg \to H$), vector boson fusion (qqH : $q\bar{q} \to H$), associated production with vector bosons (VH : $q\bar{q} \to VH$), and associated production with heavy quarks(QQH : $q\bar{q} \to Q\bar{Q}H$). Figure X.X shows the Feynman diagrams corresponding those mechanisms. Since H does not couple to gluon in ggH process it is produced via a top loop. At LHC ggH has the largest production rate due to PDF and the heaviness of top quark.

At hadron collider the hadronic cross section(σ) is calculated with parton-level cross-section ($\hat{\sigma}$) convoluted with PDF,

$$\sigma(pp \to H + X) = \sum_{i,j} \int dx_1 dx_2 f_i(x_1) f_j(x_2) \hat{\sigma}\left(ij \to H + X\right) \tag{1.29}$$

where i and j are colliding partons, x_1 and x_2 are longitudinal momentum fractions carried by i and j. Each component in the equation is subject to the following uncertainties. The partonic cross section is calculated at given a renormalizaion scale μ_R and a factorization scale μ_F. Due to possible uncalculated higher-order QCD radiative corrections, the uncertainty is estimated by varying the scales around the central values. In the de Florian and Grazzini (dFG) calculation [ref], the central values are chosen to be $\mu_0 = m_{\mathrm{H}}$. The scales μ_R and μ_F are varied are in the range $\frac{1}{2}\mu_0 < \mu_F, \mu_R < 2\mu_0$ with a constraint $\frac{1}{2} < \frac{\mu_F}{\mu_R} < 2$. PDF is obtained by fitting on data measured in deep-inelastic scattering, Drell-Yan, and jet production from

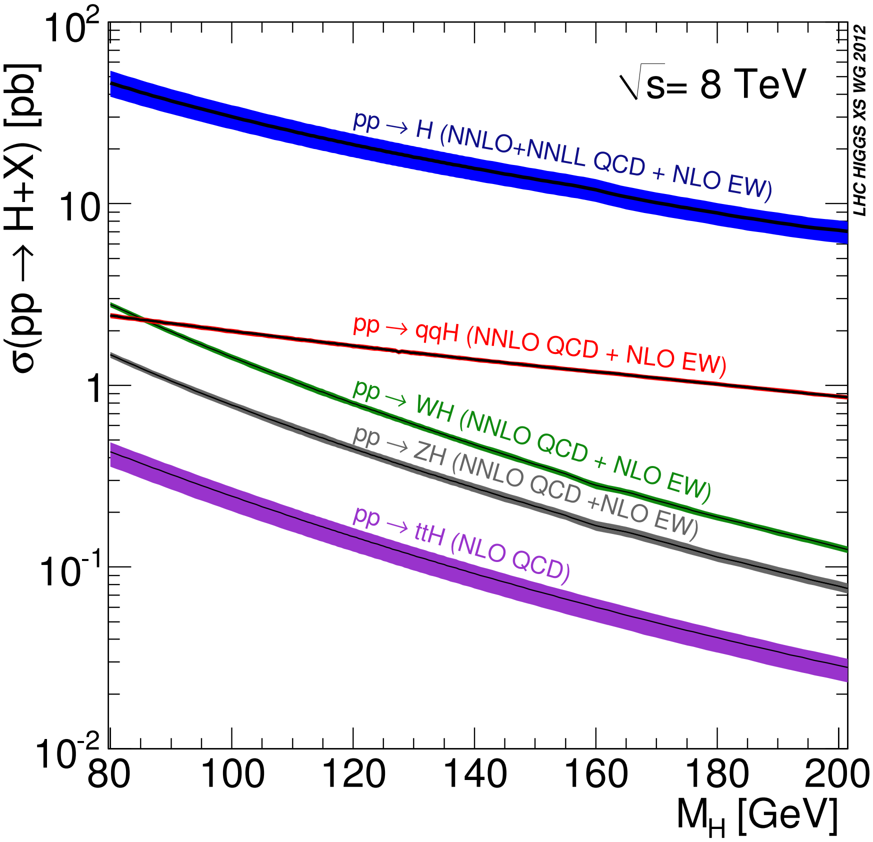

Figure 1.4: Standard model Higgs production cross sections as a function of m_{H} at $\sqrt{s} = 8$ TeV for each production mode. The ggF and VBF processes are calculated in complex-pole-scheme (CPS), while other WH/ZH and ttH processes are calculated in zero-width-approximation (ZWA).

a wide variety of different experiments. The accuracy on those data can introduce uncertainty on PDF calculation. In addition, strong coupling constant α_s is used in DGLAP evolution [ref] to the higher Q^2 region. Thus, its uncertainty also contributes to the total cross section. There are other uncertainties due to the EW corrections, the different choice of top and bottom quark masses, and the use of large-m_T method. But, the effect to the hadronic cross section is less than a few percent [?] for ggF.

Figure 1.4 shows the hadronic cross sections as a function of m_{H} for SM Higgs production and uncertainty in different production modes. The ggF and VBF cross sections are based on complex-pole-scheme (CPS), while VH and ttH ones are based on zero-width-approximation (ZWA). The order of QCD and EW

process	QCD	EW
$pp \to H$	NNLO	NLO
$pp \to qqH$	NNLO	NLO
$pp \to WH$	NNLO	NLO
$pp \to ZH$	NNLO	NLO
$pp \to ttH$	NLO	

Table 1.2: The order of QCD and EW calculations.

calculations are summarized in Table 1.2.1. The uncertainty is linear combination of uncertainties from QCD scale varitaion and PDF+α_S. At $m_{\mathrm{H}} = 125$ GeV ggH contributes $\sim 87\%$ to the total cross section.

1.2.2 Decay of Higgs Boson

The interaction term in the Lagrangian shows that the Higgs can couple to a pair of weak bosons(VV). Thus, Higgs decays into W^+W^- and ZZ. Depending on the mass of Higgs, one or two of the bosons can be off-shell. Thus we consider three cases where both of them are on-shell(VV), one is on-shell and the other is off-shell(VV^*), and both of them are off-shell(V^*V^*).

- Both bosons are on-shell($H \to VV$) [ref] :

$$\Gamma(H \to VV) = \frac{\mathrm{G_F} m_{\mathrm{H}}^3}{16\sqrt{2}\pi} \delta_V \sqrt{1-4\epsilon^2}\left(1-4\epsilon^2-12\epsilon^4\right) \tag{1.30}$$

where $\epsilon = \dfrac{M_V}{m_{\mathrm{H}}}$ and $\delta_W = 2$ and $\delta_Z = 1$. The ratio of londitudinal polarization is given by [?]

$$R_L = \frac{\Gamma_L}{\Gamma_T + \Gamma_L} = \frac{1-4\epsilon^2-4\epsilon^4}{1-4\epsilon^2-12\epsilon^4} \xrightarrow{\epsilon \to 0} 1 \tag{1.31}$$

Thus, vector bosons are longitudinally polarized at high m_{H} ($\epsilon \to 0$). At the production threshold, $m_{\mathrm{H}} = 2M_V \to \epsilon = \frac{1}{2}$, R_L is 2 which means that longitudinal and transverse polarizations are equally populated. In addition, the decay width to WW is reduced to

$$\begin{aligned} \Gamma(H \to WW) &\to \frac{\mathrm{G_F} m_{\mathrm{H}}^3}{16\sqrt{2}\pi} \times 2 && (1.32) \\ &= 2\frac{1.16637 \times 10^{-5}\ \mathrm{GeV}^{-2} m_{\mathrm{H}}^3}{16\sqrt{2}\pi} && (1.33) \\ &\approx 0.33 m_{\mathrm{H}} \times \frac{m_{\mathrm{H}}^2}{\mathrm{TeV}^2}(\mathrm{TeV}). && (1.34) \end{aligned}$$

For example, at $m_{\mathrm{H}} = 1$ TeV, decay width for WW is 0.33 TeV. Practically t is hard to claim a Higgs resonance at high mass regions.

- one is on-shell and the other is off-shell ($H \to VV^* \to Vf\bar{f}$) where f does not include top quark [ref] :

$$\Gamma(H \to VV^*) = \frac{3{\mathrm{G_F}}^2 M_v^4}{16\pi^3} m_{\mathrm{H}} \delta'_V R(\epsilon) \tag{1.35}$$

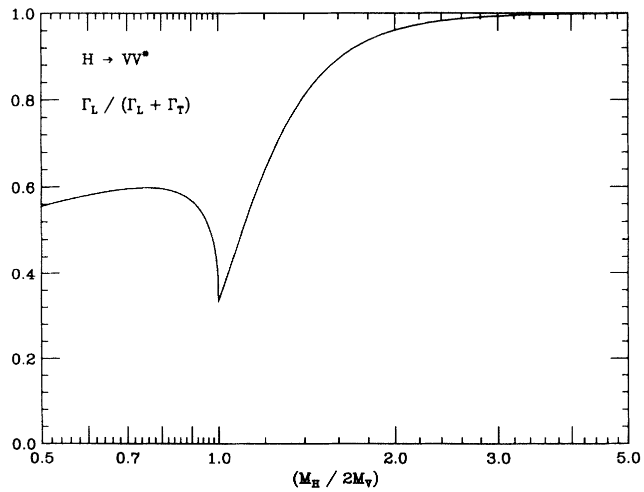

Figure 1.5: The ratio of longitudinal polarization of vector bosons as a function of $\frac{m_{\mathrm{H}}}{2M_V}$ [?]

where $\delta'_W = 1$, $\delta'_Z = \frac{7}{12} - \frac{10}{9}\sin^2\theta_W + \frac{40}{9}\sin^4\theta_W$, and

$$\begin{aligned} Rf(\epsilon) = &\frac{3(1-8\epsilon^2+20\epsilon^4)}{(4\epsilon^2-1)^{1/2}} \arccos\left(\frac{3\epsilon^2-1}{2\epsilon^3}\right) \\ &-(1-\epsilon^2)\left(\frac{47}{2}\epsilon^2 - \frac{13}{2} + \frac{1}{\epsilon^2}\right) - 3(1-6\epsilon^2+4\epsilon^4)\ln\epsilon \end{aligned} \tag{1.36}$$

The ratio of londitudinal polarization is given [?] by

$$R_L = \frac{\Gamma_L}{\Gamma_T + \Gamma_L} = \frac{R_L(\epsilon)}{R(\epsilon)} \tag{1.37}$$

where R_L is [?]

$$\begin{aligned} R_L(\epsilon) = &\frac{3(1-16\epsilon^2+20\epsilon^4)}{(4\epsilon^2-1)^{1/2}} \arccos\left(\frac{3\epsilon^2-1}{2\epsilon^3}\right) \\ &-(1-\epsilon^2)\left(\frac{15}{2}\epsilon^2 - \frac{13}{2} + \frac{1}{\epsilon^2}\right) - (3-10\epsilon^2+4\epsilon^4)\ln\epsilon. \end{aligned} \tag{1.38}$$

Figure 1.5 shows the ratio of longitudinally polarized vector bosons as a function of $\frac{m_{\mathrm{H}}}{2M_V}$ $(=\frac{\epsilon}{2})$. The ratio changes as m_{H} changes. Thus, we expect event kinematics differs with different m_{H} hypotheses. This is important when we define signal regions optimized at a given m_{H} hypothesis. mention $\Delta\phi_{ll}$ here? What does it mean that Vs are transervely polarized? (schemetically)

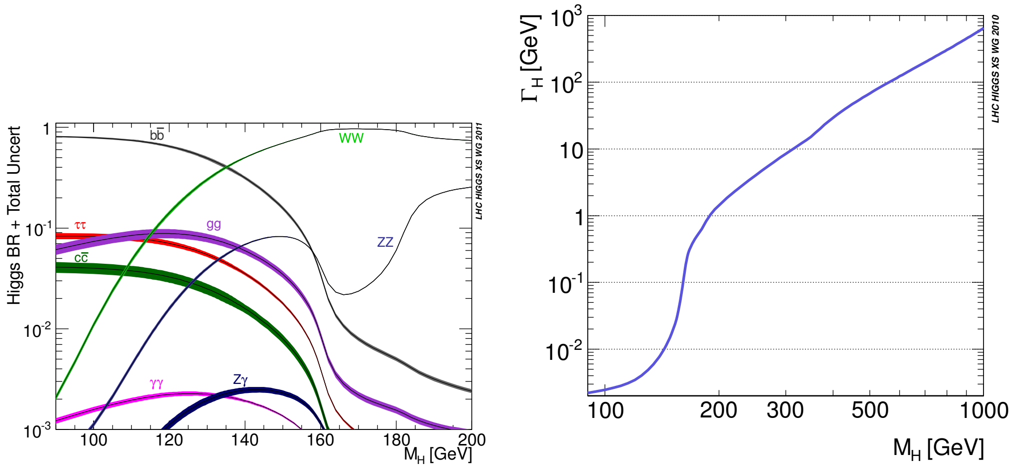

Figure 1.6: Standard Model Higgs boson decay branching ratios at low m_{H}(left) and total width (right).

Figure 1.6 shows the branching ratios of Standard Model Higgs boson and its total decay width. Top and bottom quarks are included in the calculation. Uncertainties are from ...

Figure 1.7 shows $\sigma \times BR$ at low m_{H}.

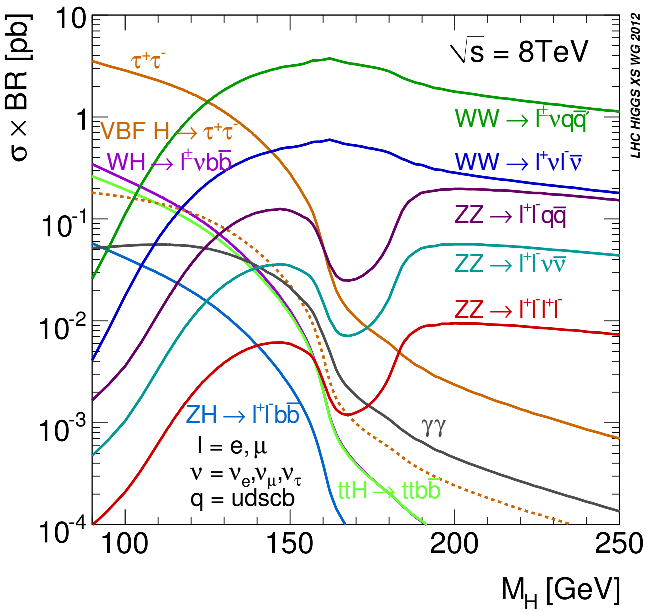

Figure 1.7: $\sigma \times BR$ at low m_{H}.

1.3 Limits on Higgs Boson Mass

1.3.1 Theoretical Limits

Perturbative Unitarity : $W_L^+W_L^- \to W_L^+W_L^-$

The cross section of longditudinal vector boson scattering, $V_LV_L \to V_LV_L$, increases as the energy increases, which eventually violate unitarity. This will be discussed in thie subsection taking $W_L^+W_L^- \to W_L^+W_L^-$ as an example. Fig. 1.8 shows Feynman diagrams for this process. In the high energy limit $s \gg m_{\mathrm{W}}^2$, the scattering amplitude is [?]

$$\mathcal{A}\left(W_L^+W_L^- \to W_L^+W_L^-\right) \sim -\frac{1}{v^2}\left(-s - t + \frac{s^2}{s - m_{\mathrm{H}}^2} + \frac{t^2}{t - m_{\mathrm{H}}^2}\right). \tag{1.39}$$

What does the point diagram correspond to in this equation? According to the Electroweak Equivalence Theorem [?] which says that at very high energy the longitudinal vector bosons can be replaced by their associated Goldstone bosons.

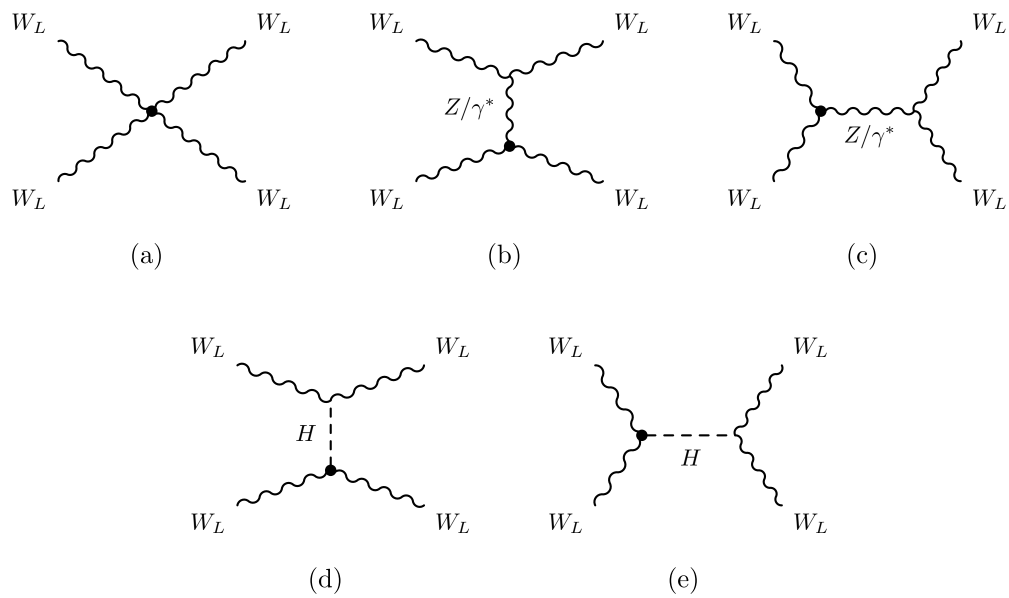

Figure 1.8: Feynman diagrams for $W_L^+W_L^- \to W_L^+W_L^-$ scattering.

Thus, the scattering amplitude can be written using Goldstone bosons ($w^\pm$)

$$\mathcal{A}\left(w^+w^- \to w^+w^-\right) = -\frac{m_{\mathrm{H}}^2}{v^2}\left(2 + \frac{m_{\mathrm{H}}^2}{s - m_{\mathrm{H}}^2} + \frac{m_{\mathrm{H}}^2}{t - m_{\mathrm{H}}^2}\right). \tag{1.40}$$

An scattering amplitude can be decomposed into partial waves a_l

$$\mathcal{A} = 16\pi \sum_{i=0}^{\infty} (2l+1)\, P_l\left(\cos\theta\right) a_l \tag{1.41}$$

where P_l is the Legendre polynominals and θ is the scattering angle. For $2 \to 2$ cross section using Optical theorem [**?**], we have the following identity on cross section (σ)

$$\sigma = \frac{16\pi}{s} \sum_{i=0}^{\infty} (2l+1) \left|a_l\right|^2 = \frac{1}{s} Im\left[\mathcal{A}\left(\theta = 0\right)\right] \tag{1.42}$$

which gives the unitary condition,

$$\left|a_l\right|^2 = Im\left(a_l\right) \qquad \Rightarrow \qquad Re\left(a_l\right)^2 + \left[Im\left(a_l\right) - \frac{1}{2}\right]^2 = \left(\frac{1}{2}\right)^2 \tag{1.43}$$

$$\Rightarrow \qquad \left|Re\left(a_l\right)\right| < \frac{1}{2}. \tag{1.44}$$

Then, the $l=0$ amplitude in the limit of $s \gg m_{\mathrm{H}}^2$ becomes

$$a_0\left(w^+w^- \to w^+w^-\right) = -\frac{m_{\mathrm{H}}^2}{16\pi v^2}\left[2+\frac{m_{\mathrm{H}}^2}{s-m_{\mathrm{H}}^2}-\frac{m_{\mathrm{H}}^2}{s}\log\left(1+\frac{s}{m_{\mathrm{H}}^2}\right)\right] \quad (1.45)$$

$$\to -\frac{m_{\mathrm{H}}^2}{8\pi v^2} \quad (1.46)$$

The unitary condition (Eq. (1.44)) gives upper bound on m_{H},

$$|Re\,(a_0)| = \frac{m_{\mathrm{H}}^2}{8\pi v^2} < \frac{1}{2} \quad (1.47)$$

$$\Rightarrow \quad m_{\mathrm{H}} < 2\sqrt{\pi}v \simeq 870 \text{ GeV}. \quad (1.48)$$

Including other scattering channels,

$$Z_L Z_L,\ \ HH,\ \ Z_L H,\ \ W_L^+ H,\ \ W_L^+ Z_L \quad (1.49)$$

the constraint on m_{H} becomes tigher [?],

$$m_{\mathrm{H}} < 710 \text{ GeV}. \quad (1.50)$$

This means that in SM unitariry will be violated if $m_{\mathrm{H}} > 710$ GeV unless there is a new physics that recovers it. So far we calculated only tree-level terms, so we can expect that adding higher order terms can solve this problem. But, including higher order terms does not gaurantee that the unitary will be restored because in the high m_{H} regime coupling to Higgs is too large and perturbative calculation breaks down. Thus, the mass bound given in eq. 1.50 can be considered the m_{H} regime where perturbative calculation is reliable in all s.

Triviality and Stability bounds

The variation of the Higgs quartic couping λ is described by Renormalization Group Equation (RGE). When we consider one-loop radiation correction by Higgs boson itself to λ which are shon in the Fig.1.9, the corresponding RGE is given by [?]

$$\frac{d}{dQ^2}\lambda(Q^2) = \frac{3}{4\pi^2}\lambda^2(Q^2) + \text{higher orders} \quad (1.51)$$

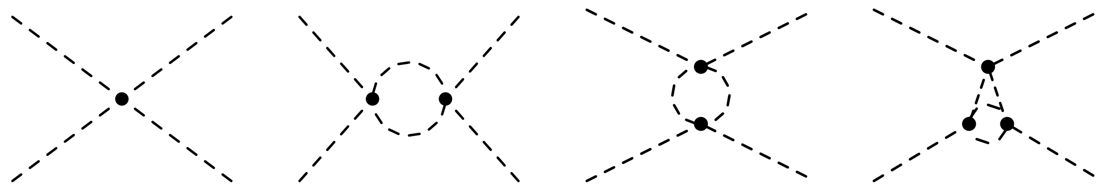

Figure 1.9: Feynman diagrams for Higgs boson quartic interaction. Left is tree lebel and the right three are one-loop correction by Higgs boson itself.

The solution to this equation is given by

$$\lambda(Q^2) = \frac{\lambda(v^2)}{\left[1 - \frac{3}{4\pi^2}\lambda(v^2)\log\frac{Q^2}{v^2}\right]} \tag{1.52}$$

where the EWSB scale is used as a reference energy point, $Q_0 = v$. If the energy is much smaller than the EWSB scale, $Q^2 \ll v^2$, the quadratic coupling goes to 0, and the theory is called "trivial", which means that there is no interaction. On the otherhand, if the energy is much larger than the EWSB scale, $Q^2 \gg v^2$, as Q increases the coupling will be infinite at a certain energy scale, Λ_{cut}. Using $\lambda = m_{\mathrm{H}}^2/2v^2$ and the defition of λ that it is positive, we have the following equation for denominator,

$$1 > \frac{3}{4\pi^2}\frac{m_{\mathrm{H}}^2}{2v^2}\log\frac{\Lambda_{cut}^2}{v^2} \qquad \Rightarrow \qquad m_{\mathrm{H}}^2 > \frac{8\pi^2 v^2}{\log\frac{\Lambda_{cut}^2}{v^2}}, \tag{1.53}$$

which gives a scale-dependent bound on m_{H}. Imposing $\Lambda_{cut} = m_{\mathrm{H}}$ in which case the theory is not reliable, i.e. valid scale of theory is same as the mass of a particle, the bound on the Higgs mass is $m_{\mathrm{H}} < 640$ GeV. This result is consistent with the limit from unitarity constraint.

In the previous discussion, only was one-loop correction by Higgs itself considered. This is a proper approximation when λ is large. But, in other cases where λ is small, we need to consider the contributions from fermions and vector bosons. Since, the strength of interaction with Higgs boson is proportional to the particle mass, we consider only heavy particles, vector bosons and top quarks. In the limit of small Higgs quartic couplings, $\lambda \ll \lambda_t, g_1, g_2$ where λ_t is the top Yukawa coupling given by $\sqrt{2}m_{\mathrm{t}}/v$, the RGE is given by [?]

$$\frac{d}{dQ^2}\lambda(Q^2) \simeq \frac{1}{16\pi^2}\left[-12\frac{m_{\mathrm{t}}^4}{v^4} + \frac{3}{16}\left(2g_2^4 + \left(g_2^2+g_1^2\right)^2\right)\right]. \tag{1.54}$$

Taking EWSB scale as the reference point, the solution to Eq. (1.54) is

$$\lambda\left(Q^2\right) = \lambda\left(v^2\right) + \frac{1}{16\pi^2}\left[-12\frac{m_{\mathrm{t}}^4}{v^4} + \frac{3}{16}\left(2g_2^4 + \left(g_2^2+g_1^2\right)^2\right)\right]\log\frac{Q^2}{v^2}. \tag{1.55}$$

As $\lambda(v^2)$ becomes small, the couping can go negative, leading the vacuum unstable. Thus, in order to maintain the stability of vacuum, $\lambda\left(Q^2\right)$ should be positive. This requirement gives

$$\begin{aligned} m_{\mathrm{H}}^2 &> \frac{v^2}{8\pi^2}\left[-12\frac{m_{\mathrm{t}}^4}{v^4} + \frac{3}{16}\left(2g_2^4 + \left(g_2^2+g_1^2\right)^2\right)\right]\log\frac{\Lambda_{cut}^2}{v^2} && (1.56)\\ &= \frac{v^2}{8\pi^2}\left[-12\frac{m_{\mathrm{t}}^4}{v^4} + \frac{3}{16}\left(2g_2^4 + \left(g_2^2+g_1^2\right)^2\right)\right]\log\frac{\Lambda_{cut}^2}{v^2} && (1.57)\\ &= \text{work on this line} && (1.58)\end{aligned}$$

So far the higher order contributions were taken up to 1-loop corrections. There are calculations upto 2-loops and Fig. 1.10 shows lower bound (vacuum stability) and upper bound (triviality) of m_{H}as a function of new cutoff scale, Λ_{cut}.

Fine tuning

The 1-loop radiative corrections to Higgs mass when only are W/Z/H and top contributions condsidered is given by [?]

$$m_{\mathrm{H}}^2 = \left(m_{\mathrm{H}}^0\right)^2 + \frac{3\Lambda_{UV}^2}{8\pi^2 v^2}\left[m_{\mathrm{H}}^2 + 2m_{\mathrm{W}}^2 + m_{\mathrm{Z}}^2 - 4m_{\mathrm{t}}^2\right] \tag{1.59}$$

where m_{H}^0 is the fundamental parameter of SM and Λ_{UV} is the UV cutoff scale. Therefore, unless Λ_{UV} is in the same scale of EWSB(100 GeV − 1 TeV), there should be an incredible fine-tuning between m_{H}^0 and the radiative correction to get m_{H} in EWSB scale. For a quantitative discussion, we first need to define what fine-tuning means. Fine-tuning is defined as the sensitivity of the weak scale to the cutoff, $|\delta m_{\mathrm{W}}^2(\Lambda_{UV})/m_{\mathrm{W}}^2|$, where δm_{W}^2 is the difference between the tree and

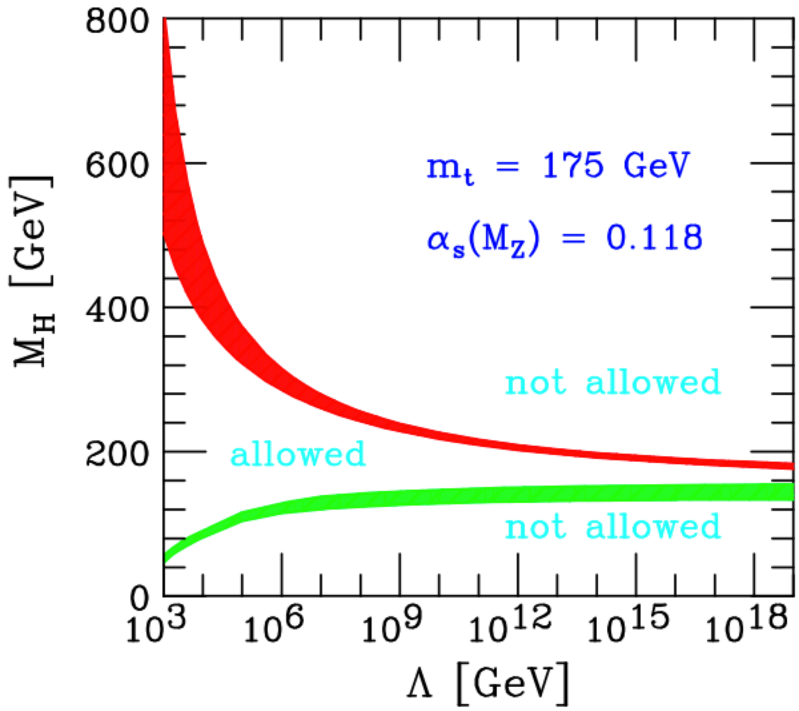

Figure 1.10: Upper and lower bound of $m_{\rm H}$as a function of Λ_{cut}.

loop values, with all other quantities held fixed [**?**]. So, the metric, $\mathcal{F}$, is

$$\mathcal{F} = \left|\frac{\delta m_{\rm W}^2}{m_{\rm W}^2}\right| = \left|\frac{\delta v^2)}{v^2}\right| = \left|\frac{\delta \mu^2}{\mu^2}\right| = \left|\frac{\delta m_{\rm H}^2}{m_{\rm H}^2}\right| = \frac{2\Lambda^2}{m_{\rm H}^2}\left|\sum_n \log^2\left(\frac{\Lambda_{UV}}{m_{\rm H}}\right)\right| \tag{1.60}$$

and $\mathcal{F} \leq 1$ represents that there is no fine-tuning. The fig. 1.11 [**?**] shows two regions in $[\Lambda, m_{\rm H}]$ plane where Λ is the UV cutoff scale, Λ_{UV}; $\mathcal{F} > 10$ in light-hatching labeled as 10 % and $\mathcal{F} > 100$ in thick-hatching labeled as 1 %. In case of light Higgs scenario, the fine-tuning is even at the low energy scale. For example, at $m_{\rm H}$=130 GeV the fineo-tuning of $\mathcal{F} > 10$(10 %) requires $\Lambda < 2.3$ TeV. This means that new physics should exist in the regime where LHC experiements can probe.

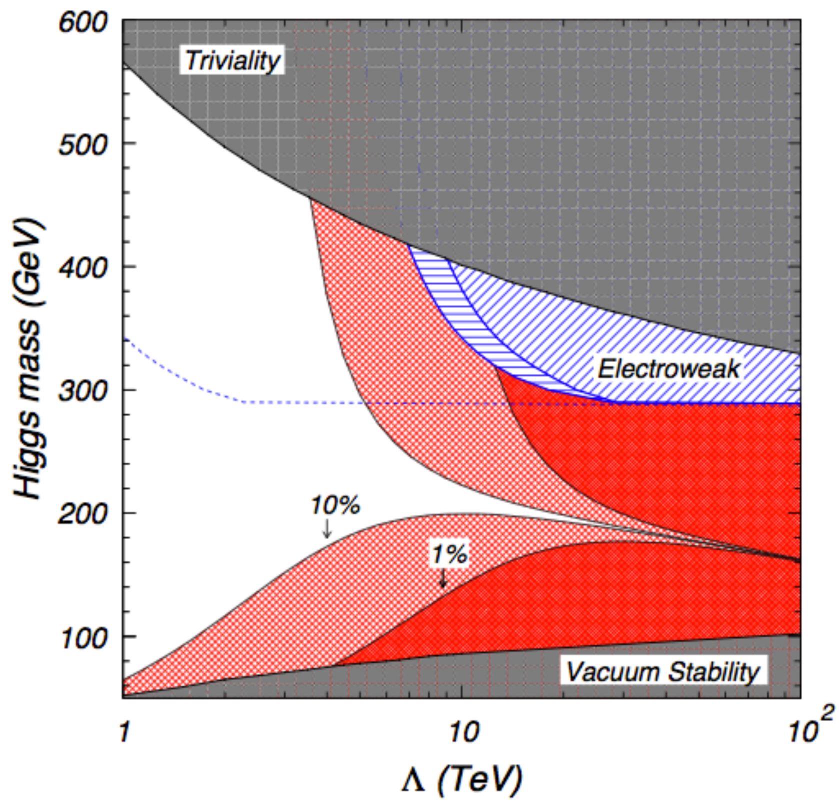

Figure 1.11: Constraint contour from fine tuning, vacuum stability, and triviality

.

1.3.2 Experimental Limits

Indirect search

There are EWK measurements that are dependent on m_{H}. For example, the mass of W boson has one-loop correction of Higgs boson as shown in Fig. 1.12. Its contribution to the W mass is parametrized by Δr in the following equation

$$m_{\mathrm{W}}^2 = \frac{\pi\alpha}{\sqrt{2}\mathrm{G_F}} \frac{1}{\left(1 - \frac{m_{\mathrm{W}}^2}{m_{\mathrm{Z}}^2}\right)} \left(1 + \Delta r\right), \tag{1.61}$$

and the correction is

$$\Delta r \simeq \frac{\mathrm{G_F} m_{\mathrm{W}}^2}{8\sqrt{2}\pi^2} \frac{11}{3} \left(\log \frac{m_{\mathrm{H}}^2}{m_{\mathrm{W}}^2} - \frac{5}{6}\right) \tag{1.62}$$

which is depedent on m_{H} logarithmically. Thus, by measuring other quantities in the equation, we can constrain m_{H} up to the uncertainties to the measured

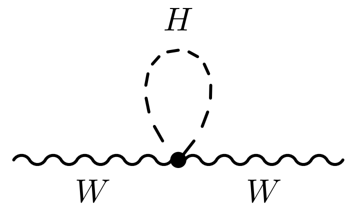

Figure 1.12: Feynman diagram for 1 loop correctioin by Higgs boson to the W propagator.

.

quantities. Going one step further, we can use more variables, not only m_{W}, and put them into a statisitcal fit [**?**]. A simultaneous fit is done to $\Delta\alpha^{(5)}_{had}(m^2_{\mathrm{Z}})$, $\alpha_S(m^2_{\mathrm{Z}})$, m_{Z}, m_{t}, and $\log_{10}(m_{\mathrm{H}})$ on the data collected by LEP-I/II, SLD, and Tevatron [**?**]. The fig. 1.13 shows $\Delta\chi^2$ curve from EWK precision measurements assuming that Standard Model is the true theory of nature [**?**]. The prefered m_{H} is 94^{+29}_{-24} GeV. It also shows that the upper limit on m_{H}at C.L. = 95 % is 152 GeV.

Direct search

Before 2012, there were direct searches for SM Higgs boson by LEP, Tevatron, and LHC experiments. The LEP data showed upper limit of $m_{\mathrm{H}} < 114.4$ GeV at CL_{s}= 95 % [**?**] and the Tevatron showed exclusion of SM Higgs hypothesis in the range of 147 GeV $< m_{\mathrm{H}} <$ 179 GeV at CL_{s}= 95 % [**?**]. At the end of 2011, the LHC experiments(CMS and ATLAS) showes their 7 TeV results on the standard model Higgs search [**?**, **?**]. Fig. 1.14 shows the 95% C.L. upper limits on $\sigma/\sigma_{\mathrm{SM}}$ as a function of m_{H} in the range of 110 - 145 GeV for CMS on the left and 110 - 150 GeVfor ATLAS on the right. In both experiments, search was performed up to m_{H}= 600 GeV, but only low m_{H} region is shown on the plots. In CMS, the observed exclusion range is 118 - 543 GeV with expected exclusion range is 127 - 600 GeV. In ATLAS, the observed exclusion range is 112.9 - 115.5, 131-238, and 251-466 GeV with expected exclusion range 124 - 519 GeV. Both experiments, CMS and ATLAS, show local excess of 3.1σ and 3.5σ, repectively, around m_{H}= 125 GeV

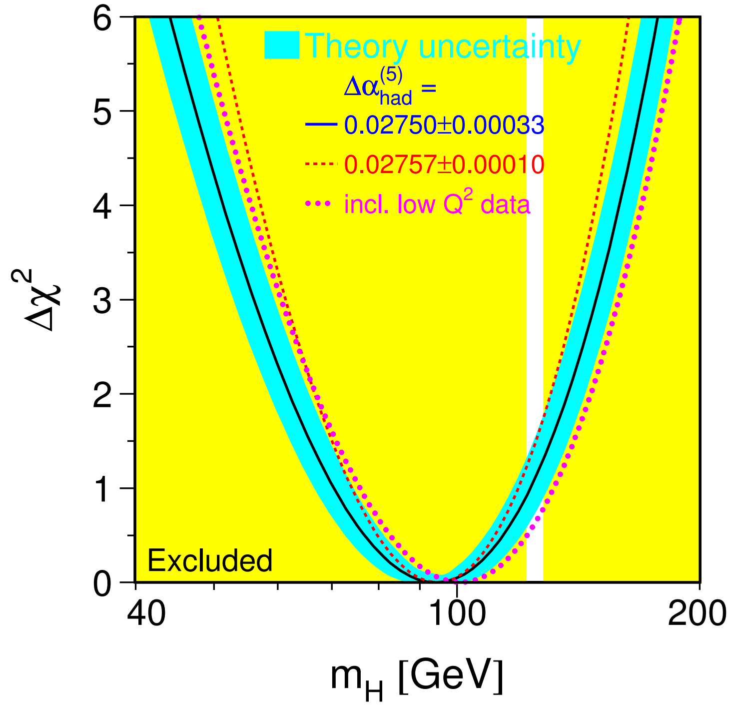

Figure 1.13: blah

1.4 $H \to W^+W^- \to 2l2\nu$

1.4.1 Large expected signal yields

As seen in the previous section, the $\sigma \times$BR of $H \to W^+W^- \to 2l2\nu$ channel is large compared to the other sensitive channels, $H \to ZZ \to 4l$ and $H \to \gamma\gamma$. Table 1.4.1 shows $\sigma \times$ BR for the most sensitive channels, $H \to W^+W^- \to 2l2\nu$,

	$H \to WW \to 2l2\nu$	$H \to ZZ \to 4l$	$H \to \gamma\gamma$
$\sigma \times BR(pb)$	2.24×10^{-1}	2.79×10^{-3}	5.09×10^{-2}
$N_{expected}$ in $\mathcal{L}_{int} = 20$ fb^{-1}	4480	56	1018

Table 1.3: $\sigma \times BR$ at $m_{\rm H} = 125$ GeV for most sensitive channels and the expected number of events in $\mathcal{L}_{int} = 20$ fb^{-1}. l means electrons or muons.

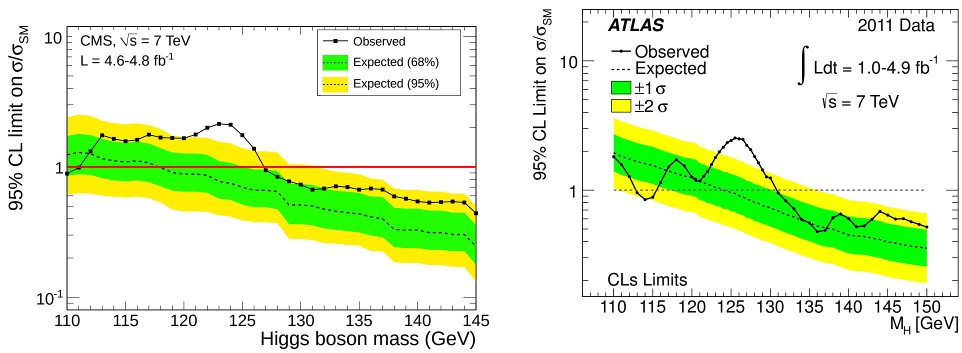

Figure 1.14: CMS / ATLAS Higgs exclusion with 7 TeV data.

$H \to ZZ \to 4l$, and $H \to \gamma\gamma$ and the expected signal events at the integrated luminosity, $\mathcal{L} = 20\ \text{fb}^{-1}$. The expected signal events are 4480, 56, and 1018, respectively. This allows to have a good statistical power to measure the cross section (signal strength) with this channel.

1.4.2 Angular distribution of leptons in the final state

The spin of SM Higgs is zero, so by helicity conservation the total spin of the WW system should be zero. As shown in Fig. 1.15, if we take the direction of W^+ momentum as z axis in the CM of Higgs, there are two cases where the spin direction is parellel to the momentum direction (transverse polarization) and one case where it is perpendicular to the momentum direction(longitudinal polarization). In case of transverse polarization, the leptons from Ws have strong angular dependence due to V-A nature of weak decays, i.e. neutrinos are always left-handed(anti-neutrinos are always right-handed). Let's take the case of W^+ spin in the z direction as an example. In order for the neutrino from W^+ to be left-handed, the direction of the neutrino should be in the - z direction, thus lepton should fly to z direction. In order for the anti-neutrino from W^- to be right-handed, the direction of the anti-neutrino should be in the - z direction, thus lepton should fly to z direction. Therefore, both leptons tend so move in the same direction resulting the angle between the two leptons to be small. This is somewhat diluted due to boost of Higgs and Ws, but the effect is still visible and used

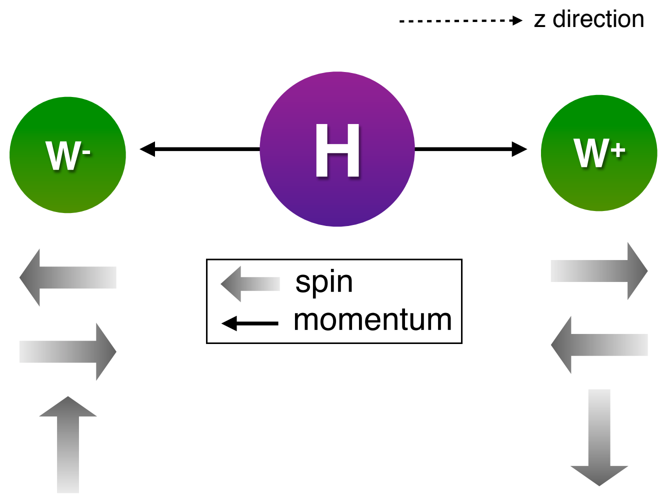

Figure 1.15: blah

to separate signals from non-resonant WW background. On the other hand, in case of longitudinal polarization, no specific angular correlation is present.

1.4.3 Kinematic variables

Figure 1.16 shows distributions of kinematic variables for multiple Higgs hypotheses, $m_{\mathrm{H}} = 110, 125, 145, 160, ,$ and 200 GeV. The plotted variables are leading and trailing lepton p_{T}, azimuthal angle difference between the two leptons $\Delta\phi_{\ell\ell}$, di-lepton invariant mass $m_{\ell\ell}$, and Higgs transverse mass m_{T} which is defined as

$$m_{\mathrm{T}} = \sqrt{2p_{\mathrm{T}}^{\ell\ell}E_{\mathrm{T}}^{\mathrm{miss}}(1 - cos(\Delta\phi_{\ell\ell - E_{\mathrm{T}}^{\mathrm{miss}}}))} \tag{1.63}$$

where p_{T} is transverse momentum of the dilepton system, $E_{\mathrm{T}}^{\mathrm{miss}}$ is missing transverse momentum, and $\Delta\phi_{\ell\ell - E_{\mathrm{T}}^{\mathrm{miss}}}$ is the angle between dilepton direction and $E_{\mathrm{T}}^{\mathrm{miss}}$ in the transverse plane. The most of events have leading lepton $p_{\mathrm{T}}^{\ell,\mathrm{max}}$ greater than 20 GeV for all m_{H} hypotheses. The The trailing lepton $p_{\mathrm{T}}^{\ell,\mathrm{min}}$ is quite populated at low $p_{\mathrm{T}}^{\ell,\mathrm{min}}$ region, especially for low m_{H} hypotheses. In case of m_{H}= 125 GeV, approximately 25 % of events are rejected by requiring $p_{\mathrm{T}}^{\ell,\mathrm{min}} > 10$ GeV. The

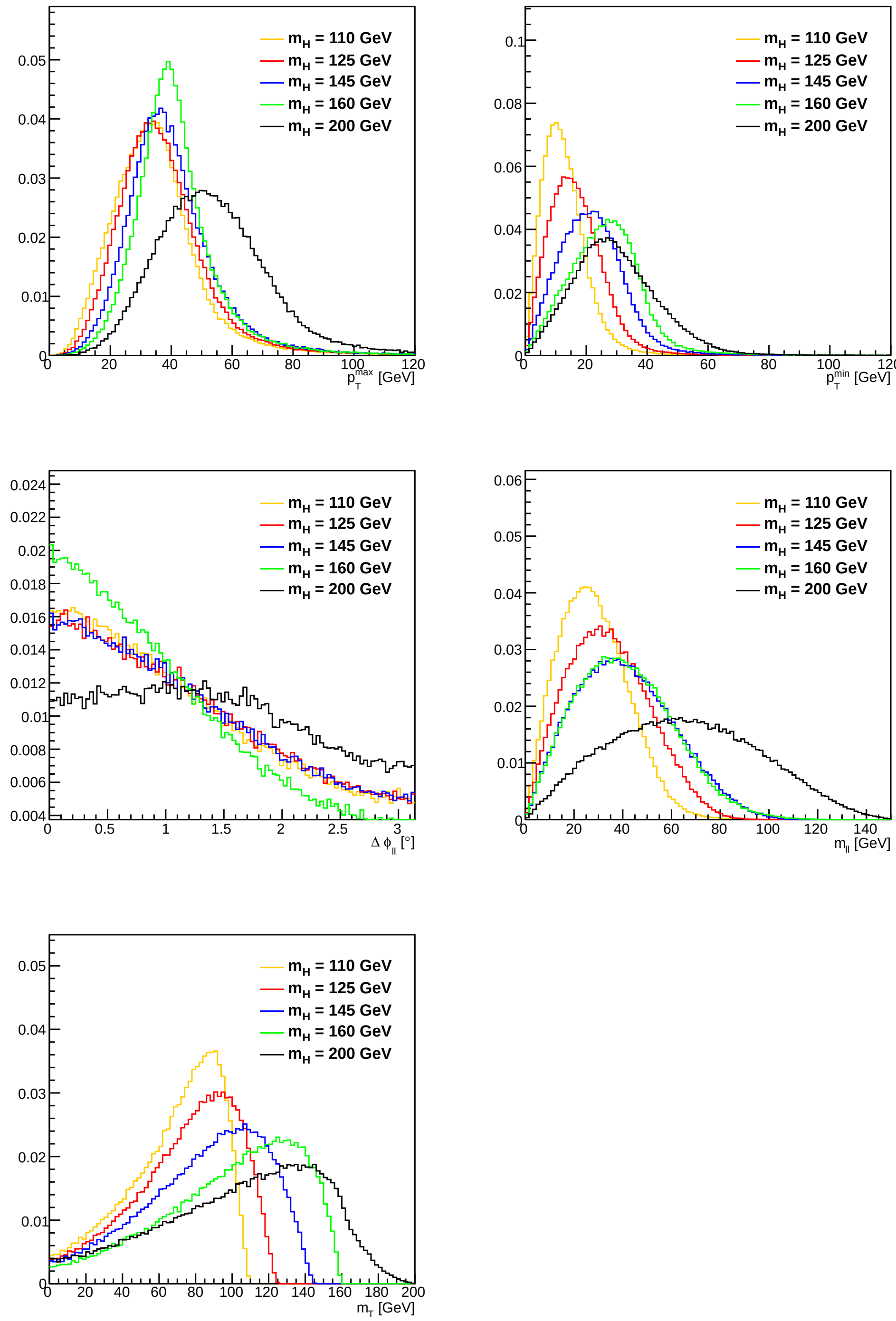

Figure 1.16: blah

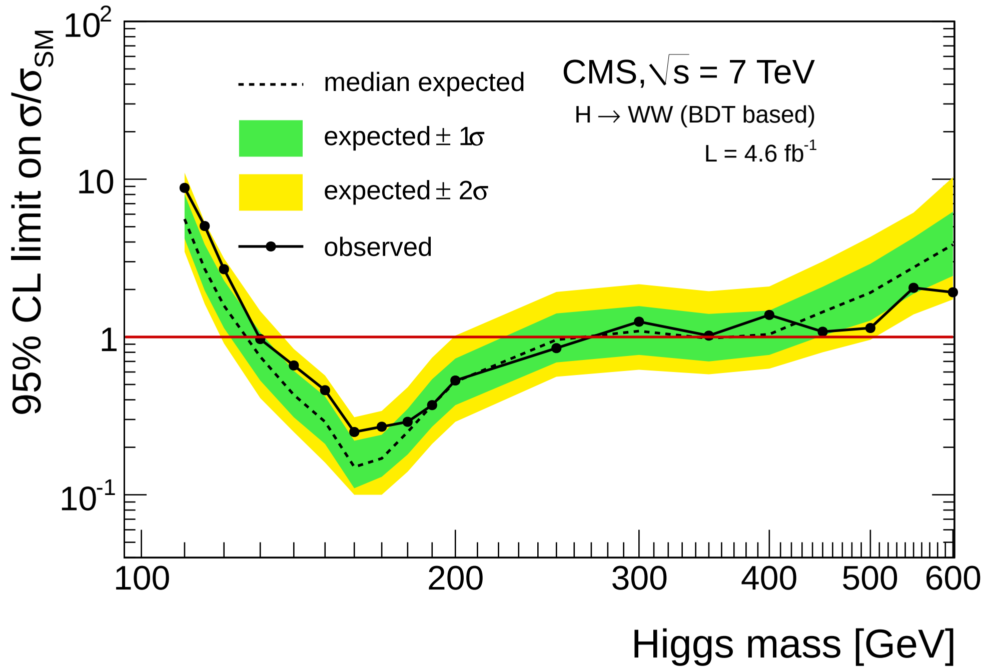

Figure 1.17: Exclusion limit of SM Higgs with 2011 data($\sqrt{s}$ = 7 TeV, $\mathcal{L}$ = 4.6 fb^{-1}). The observed(expected) exclusion limit at CL = 95 % is m_{H}= 129 - 270(127 - 270) GeV.

$\Delta\phi_{\ell\ell}$, azimuthal angle differece between the two leptons, shows non-straightforward trend. The angle tends to get smaller as m_{H} increases up to 160 GeV, and the angle becomes wide after m_{H}= 160 GeV. This behavior was expected in the fig. 1.5 where the fraction of the longitudinal polarization is at the minimum at m_{H}= $2m_{\mathrm{W}}$ which is about 160 GeV. Since small $\Delta\phi_{\ell\ell}$ yields small $m_{\ell\ell}$, we expect small $m_{\ell\ell}$ for low m_{H}hypotheses. The Higgs transverse mass m_{T} shows clear drop at m_{H}why tail and lazy drop at 200 GeV?,

1.4.4 CMS HWW results as of 2011

Before 2012, 4.6 fb^{-1} of data at $\sqrt{s}$ = 7 TeV collected by CMS detector was analyzed for SM Higgs search [?]. Figure 1.17 shows exclusion limit using the state-of-the-art analysis technique at the time of study. The observed exclusion limit at CL_{s}= 95 % is m_{H}= 129 - 270 GeVwith expected limit m_{H}= 127 - 270 GeV.

Chapter 2

LHC and CMS Detector

Chapter 3

Event Reconstruction and Selection

Chapter 4

Signal Extraction

Chapter 5

Efficiency Measurements

Chapter 6

Background Estimation

Chapter 7

Systematic Uncertainty

Chapter 8

Fit Validation

Chapter 9

Statistical Interpretation

Chapter 10

Results

Chapter 11

Study on Spin-Parity of the New Boson

Appendix A

Some Details on Statistical Procedure

Appendix B

More 2D templates

Bibliography

[1] CMS Collaboration. *CMS Physics: Technical Design Report Volume 1: Detector Performance and Software.* Technical Design Report CMS. CERN, Geneva, 2006. There is an error on cover due to a technical problem for some items.

[2] Ioana Anghel. Status of the CMS silicon strip tracker and commissioning results. *Nuclear Instruments and Methods in Physics Research Section A: Accelerators, Spectrometers, Detectors and Associated Equipment*, 604(12):277 – 280, 2009.

[3] D. Abbaneo. Layout and performance of the CMS silicon strip tracker. *Nuclear Instruments and Methods in Physics Research Section A: Accelerators, Spectrometers, Detectors and Associated Equipment*, 518(12):331 – 335, 2004.

[4] S Chatrchyan et al. Performance of CMS hadron calorimeter timing and synchronization using test beam, cosmic ray, and lhc beam data. *JINST*, 5:T03013, 2010.

[5] Min Suk Kim et al. CMS reconstruction improvement for the muon tracking by the rpc chambers. *PoS*, RPC2012:045, 2012.

[6] Silvia Maselli. Calibration of the barrel muon drift tubes system in CMS. Technical Report CMS-CR-2009-100, CERN, Geneva, May 2009.

[7] Thomas Lenzi. Development and study of different muon track reconstruction algorithms for the level-1 trigger for the CMS muon upgrade with gem detectors. 2013.